

Bis-sulfonamido-2-phenylbenzoxazoles Validate the GroES/EL Chaperone System as a Viable Antibiotic Target

Jack Godek,[#] Jared Sivinski,[#] Edmond R. Watson,[#] Felicidad Lebario, Wenli Xu, Mckayla Stevens, Christopher J. Zerio, Andrew J. Ambrose, Xiaoyi Zhu, Carlee A. Trindl, Donna D. Zhang, Steven M. Johnson, Gabriel C. Lander,^{*} and Eli Chapman^{*}



Cite This: *J. Am. Chem. Soc.* 2024, 146, 20845–20856



Read Online

ACCESS |



Metrics & More



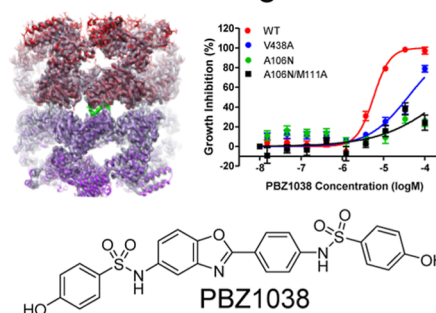
Article Recommendations



Supporting Information

ABSTRACT: We recently reported on small-molecule inhibitors of the GroES/GroEL chaperone system as potential antibiotics against *Escherichia coli* and the ESKAPE pathogens but were unable to establish GroES/GroEL as the cellular target, leading to cell death. In this study, using two of our most potent bis-sulfonamido-2-phenylbenzoxazoles (PBZs), we established the binding site of the PBZ molecules using cryo-EM and found that GroEL was the cellular target responsible for the mode of action. Cryo-EM revealed that PBZ1587 binds at the GroEL ring–ring interface (RRI). A cellular reporter assay confirmed that PBZ1587 engaged GroEL in cells, but cellular rescue experiments showed potential off-target effects. This prompted us to explore a closely related analogue, PBZ1038, which is also bound to the RRI. Biochemical characterization showed potent inhibition of Gram-negative chaperonins but much lower potency of chaperonin from a Gram-positive organism, *Enterococcus faecium*. A cellular reporter assay showed that PBZ1038 also engaged GroEL in cells and that the cytotoxic phenotype could be rescued by a chromosomal copy of *E. faecium* GroEL/GroES or by expressing a recalcitrant RRI mutant. These data argue that PBZ1038's antimicrobial action is exerted through inhibition of GroES/GroEL, validating this chaperone system as an antibiotic target.

Antibiotic action through GroEL inhibition



INTRODUCTION

GroEL, an 800 kDa homotetradecameric ATP-dependent chaperone, along with its 70 kDa homoheptameric cochaperone, GroES, assists in the folding of newly translated and stress-denatured proteins. GroEL is arranged as a back-to-back protomer, with only one of the two rings participating in refolding tasks at a time due to nested allostery [Monod–Wyman–Changeux within each GroEL ring and Koshland–Nemethy–Filmer (KNF) between GroEL rings].^{1–10} While the GroES/GroEL chaperone system is thought to assist in the refolding of approximately 10% of the *Escherichia coli* proteome, more than a dozen essential proteins require this chaperone system for their initial folding or refolding after stress—a function that cannot be compensated for by other classes of molecular chaperones.^{1–3,5,8} As a result, GroES and GroEL are themselves essential proteins, and loss of expression or function leads to bacterial cell death.^{2,11} Thus, we have been exploring GroES/GroEL chaperonins as antimicrobial targets and have identified and derivatized numerous inhibitors against them, many of which exhibit potent and selective antibacterial effects in liquid culture.^{12–14}

The ESKAPE pathogens (divided into Gram-positive pathogens *Enterococcus faecium* and *Staphylococcus aureus* and

Gram-negative pathogens *Klebsiella pneumoniae*, *Acinetobacter baumannii*, *Pseudomonas aeruginosa*, and *Enterobacter* species) make up the most common healthcare-associated antibiotic-resistant bacteria. It is estimated that millions of people become infected with these pathogens, leading to the deaths of tens of thousands every year in the USA alone.^{15,16} The discovery of new antimicrobials to treat these diseases represents an unmet need as only one mechanistically unique antibiotic has been introduced to the clinic in the last 20 years, and its effectiveness is limited only to the Gram-positive ESKAPE pathogens.^{17–19} The GroES/GroEL chaperone system is known to be essential for the survival of both Gram-negative and Gram-positive ESKAPE pathogens,^{20–25} so we aim to develop a new class of inhibitors targeting GroES/GroEL in these bacteria. We previously screened approximately 700,000 molecules against the *E. coli* GroES/GroEL

Received: April 12, 2024

Revised: July 13, 2024

Accepted: July 16, 2024

Published: July 23, 2024



system, an effective surrogate for canonical GroES/GroEL chaperonins, and characterized changes in the refolding activity of these chaperones.²⁶ Potent inhibitors were subsequently evaluated for their ability to inhibit the survival of *E. coli* and other medically relevant pathogens, including the ESKAPE pathogens.¹³ Our most potent derivatives (from the sulfonamido-2-arylbenzoxazole scaffold series of compounds) inhibit the growth of *E. coli* when the AcrA-TolC-AcrB efflux system is disrupted, as do some ESKAPE pathogens, but despite the high sequence similarity between their GroES/GroEL chaperone systems, uniform inhibition was not observed.^{12,27} Disruption of the AcrA-TolC-AcrB efflux system was required in *E. coli* to allow compound accumulation as it was discovered that the phenylbenzoxazole (PBZ) compounds are substrates of this system. Several testable hypotheses could explain these effects: variable penetration and/or accumulation of inhibitors within each pathogen, off-target effects, differing on-target engagement due to sequence variance among the molecule-binding sites of these homologues, or differences modulating GroEL allostery and related functional activities.

We first expressed and characterized GroES/GroEL protein complexes from the ESKAPE pathogens^{27,28} to later test whether molecule inactivity against some of the ESKAPE pathogens was due to suboptimal engagement of their GroES/GroEL chaperone systems. The ATPase and refolding rates for each GroES/GroEL system (except *S. aureus* GroES/GroEL, which could not be expressed) along with the complicated nested allostery exhibited by GroEL^{4,6,7,9,10} were analyzed.²⁸ Although differences were noted for allosteric transition points and ATPase rates between the ESKAPE pathogen and *E. coli* GroES/GroEL, our observations suggest that the mechanism of ESKAPE GroES/GroEL-client refolding for each ESKAPE pathogen is like that of the most well-studied homologue, *E. coli* GroES/GroEL. Furthermore, size-exclusion chromatography coupled with multiangle light scattering, native polyacrylamide gel electrophoresis (PAGE), charge detection mass spectrometry,^{29,30} and/or negative stain EM supported that each ESKAPE pathogen GroEL maintained a tetradecameric, 800 kDa, back-to-back double ring chaperone form similar to *E. coli* GroEL.²⁸

PBZ1587 (Figure 1), a derivative from the sulfonamido-2-arylbenzoxazole scaffold series, is one of our most potent inhibitors of *E. coli* GroES/GroEL refolding activity.^{12,31} Through a series of structural, biochemical, and biological methods, we demonstrate how key amino acid differences within this binding site of Gram-negative GroELs resulted in reduced potency against Gram-positive (*E. faecium*) GroEL. However, mode of action studies in *E. coli* revealed potential off-target effects from PBZ1587, so we turned our attention to another potent compound from this class, PBZ1038. Biochemical and modeling studies support that PBZ1038 also binds the ring–ring interface (RRI), and genetic and chemical biological studies show that PBZ1038 engages GroEL in bacteria and that this is the primary mechanism of its antibiotic action. Overall, this study outlines the activity profiles of two PBZ compounds and provides strong evidence that the PBZ1038 engagement of GroES/GroEL in bacteria leads to antibiotic activity. These observations, along with past genetic data, provide a sound basis for targeting GroES/GroEL as an antibiotic development strategy.

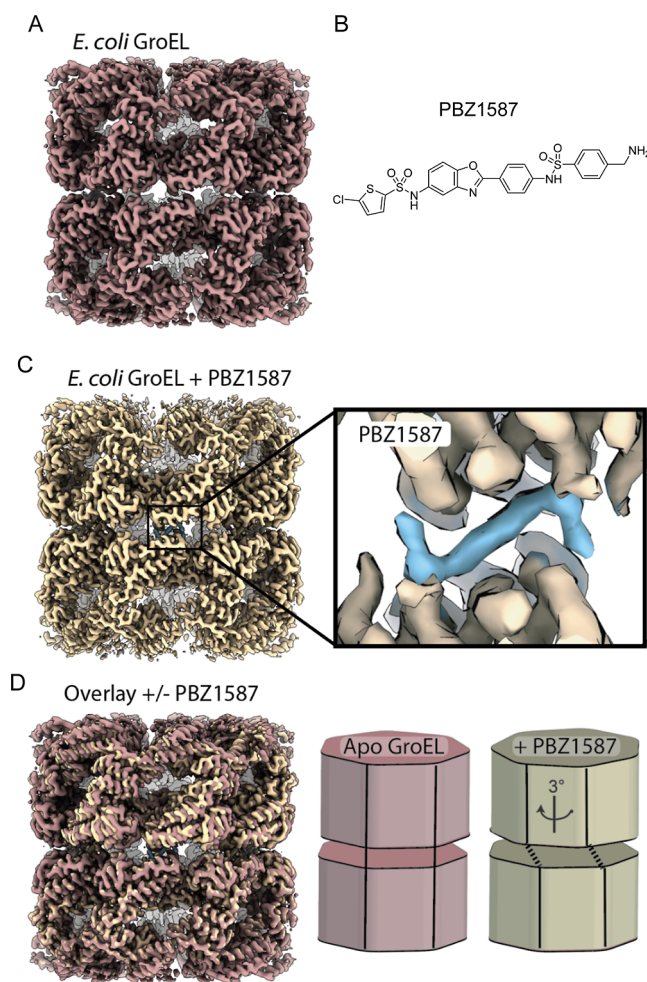


Figure 1. Cryo-EM reveals that PBZ1587 binds at the RRI of *E. coli* GroEL. (A) *E. coli* GroEL apo structure (PDB ID 9C0C). (B) Structure of PBZ1587. (C) *E. coli* GroEL + PBZ1587 bound at RRI (PDB ID 9C0B). Right, PBZ1587 density is shown. (D) Overlay of *E. coli* GroEL \pm PBZ1587, aligned on the bottom protomer. Right, graphic illustration of the protomer twist upon ligand binding. All samples were set up with a 20-fold molar excess of PBZ1587.

RESULTS AND DISCUSSION

Cryo-EM Reveals That PBZ1587 Binds at the RRI of *E. coli* GroEL. We previously identified and developed a series of bis-sulfonamido-2-PBZ compounds that provided some of our most potent GroES/GroEL inhibitors to date based on the biochemical ATPase and refolding activity of *E. coli* GroES/GroEL.^{12,31} Among these compounds, PBZ1587 exhibited antibacterial effects in *E. coli*; however, it remained unresolved whether the inhibitor was functioning on-target against GroES/GroEL. To rectify this gap in knowledge, we performed cryogenic electron microscopy (cryo-EM) to visualize where PBZ1587 binds to *E. coli* GroEL (Figure 1, Tables S1 and S2). Comparing our 3.4 Å apo GroEL structure (PDB ID 9C0C) from *E. coli* to our 3.3 Å liganded structure (PDB ID 9C0B) reveals a high-occupancy density consistent with the size and structure of PBZ1587 at all seven inter-ring contact points of the RRI (Figures 1A–C and S1). Association of the ligand also induces a noticeable $\sim 3^\circ$ interprotomer twist, seemingly disrupting ring–ring communication (KNF-type allostery) required in the refolding process (Figure 1D).

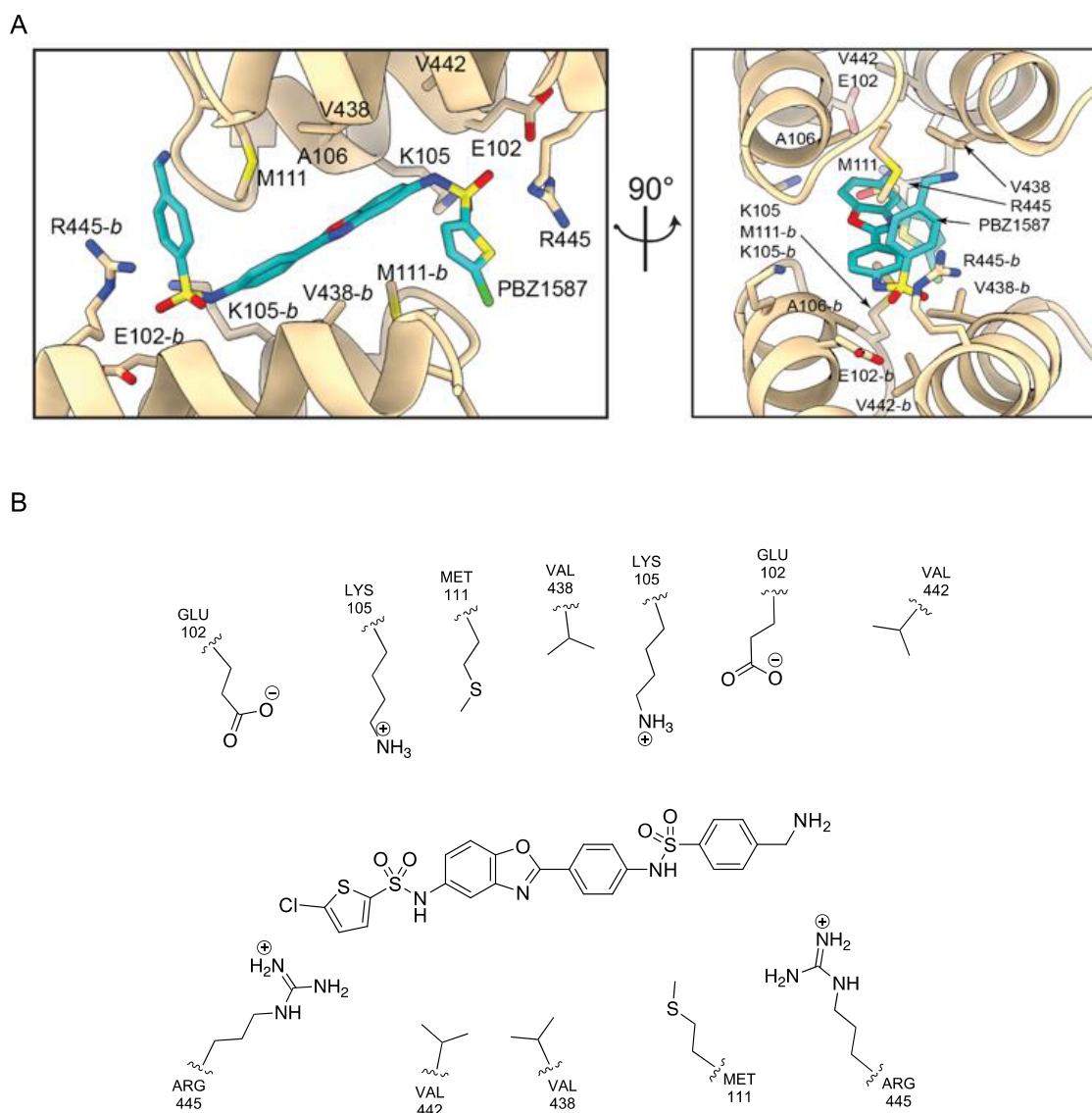


Figure 2. *E. coli* GroEL residue interactions with PBZ1587. (A) Two closeup views of the PBZ1587 binding site at the RRI of *E. coli* GroEL derived from the cryo-EM structure (PDB ID 9C0B). *E. coli* GroEL residues from both protomers are shown (identical six amino acids per protomer with residues on protomer “-b” labeled to distinguish these amino acids from the opposing monomer). (B) Predicted interactions of the *E. coli* GroEL residue with PBZ1587. Pink spheres represent amino acids on the “-b” protomer in Figure 2A. Green spheres represent amino acids on the opposing protomer in Figure 2A. Red spheres indicate theoretical water molecules. Dashed lines indicate potential residue–molecule interactions and are not to scale. See Table S3 for interaction distances and residue movements measured with PyMOL (apo vs liganded cryo-EM structures).

E. coli GroEL Residue Interactions with PBZ1587.

Because GroEL is a homotetradecamer, the residues at each of the seven ring–ring intercontact points are identical. Each interface consists of two opposing monomers (one from each protomer) within close contact (GroEL equatorial domains make up this back-to-back structure). At the RRI, PBZ1587 interacts with up to a dozen adjacent residues (Figure 2A) including van der Waals interactions between M111, V438, and V442 side chains with the PBZ scaffold core; cation–pi interactions between R445 and the benzylamine and thiophene chloride end-capping aryls; and likely hydrogen bonding and/or charge–charge interaction between the E102 and K105 side chains with the sulfonamide linkers through a theoretically ordered water molecule. While A106 is present within the binding site, it does not appear to be within the range of participating in van der Waals interactions with PBZ1587.

Changes in PBZ1587-Mediated Inhibition of MDH Refolding Assay Activity with PBZ1587-GroEL Binding-Site Mutants Support Cryo-EM Binding-Site Data.

Ten GroEL mutants were constructed to determine whether *E. coli* GroEL residues in close contact with PBZ1587 by cryo-EM are important for the PBZ1587-GroEL interaction. PBZ1587 was tested in our established biochemical GroEL refolding assay using malate dehydrogenase (MDH) as the enzymatic reporter being refolded by the chaperonin system. Mutations made to disrupt the potential GroEL-PBZ1587 interactions included: E102A and K105A (to abolish hydrogen bonding and charge–charge interactions); M111A, V438A, V438G, V442A, and V442G (to abolish or diminish van der Waals interactions); V438L and V442L (to determine if these van der Waals contacts could be strengthened by optimizing the bond distances or abolished by repulsive forces due to steric effects); and R445A (to abolish the cation–pi interactions); see Figure

2 and Table S3 for the proposed interactions. The M111A and V438G GroEL mutants were found to be lethal to *E. coli* (dominant-negative) and thus could not be recombinantly expressed. We assumed that these mutants destabilized the RRI of GroEL or otherwise hindered GroEL refolding activity to levels incompatible with cellular survival. Of the remaining eight GroEL mutants, none exhibited dominant-negative effects; thus, we were able to obtain a folding-functional chaperone to examine whether any of the mutations exhibited resistance to the inhibitory effects of PBZ1587 (Figure S2). IC₅₀ values with PBZ1587 were at least 10-fold weaker for E102A, K105A, R445A, V438A, and V442G GroEL mutants in the refolding assay compared to those of WT GroEL (Figure 3A,B).

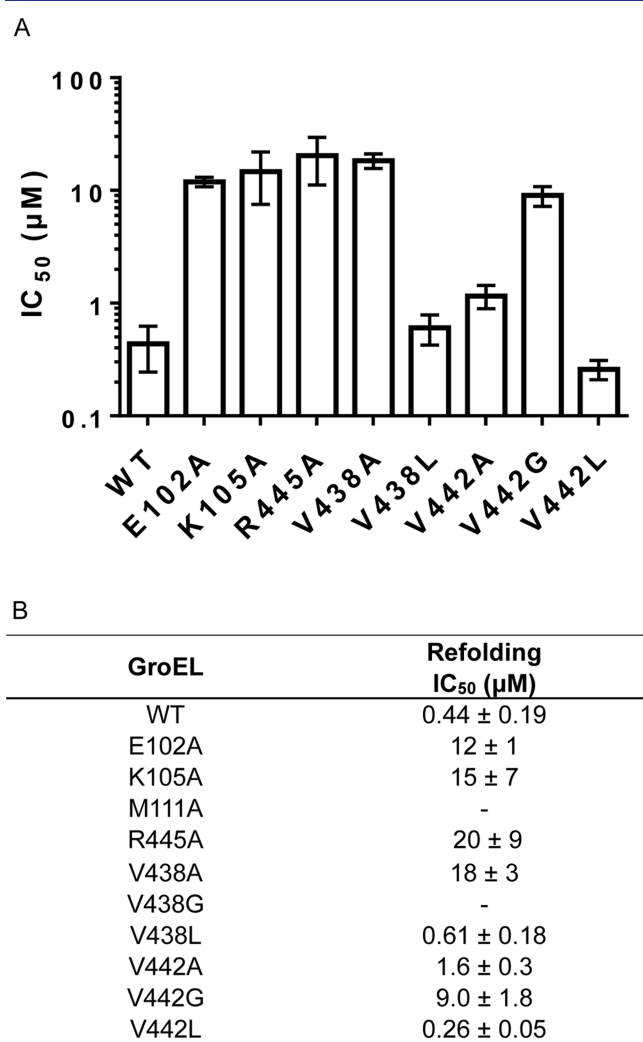


Figure 3. Changes in PBZ1587-mediated inhibition of MDH refolding assay activity with PBZ1587-GroEL binding site mutants support cryo-EM PBZ1587 binding site data. (A) PBZ1587-mediated inhibition of refolding activity for WT and mutant GroEL. WT *E. coli* GroES was included in each refolding experiment. (B) Tabulated values from (A). All experiments were performed in triplicate, and errors were expressed as the standard error of the mean (SEM). Rapid cell death was observed with M111A and V438G GroEL expression (dominant-negative) and could not be studied. All measurements were made with a 3-fold dilution series of PBZ1587 from 0.1 mM to 1.7 nM.

These data indicate that the highlighted residue interactions with PBZ1587 are critical for binding or inhibition of chaperonin activity. The E102A and K105A mutations are responsible for the loss of hydrogen bonding interactions, whereas the R445A mutations result in the loss of cation-π interactions (Figure 2 and Table S3). Critical van der Waals interactions between PBZ1587 and V438 and V442 have also been lost or diminished with V438A and V442A mutations due to the increased GroEL-PBZ1587 interaction distance. We predict that the longer hydrophobic side chains of the V438L and V442L GroEL mutants allow van der Waals contact with PBZ1587 to be maintained (compared to the alanine mutant counterparts) (Figures 2 and 3 and Table S3). Furthermore, decreased sensitivity to PBZ1587 with the V442G mutant may be explained by the lack of a hydrophobic interaction with PBZ1587 or increased flexibility of the amino acid at this position. In all, these data validate the GroEL-PBZ1587 binding site interactions, as identified in the cryo-EM structure.

E. coli and Gram-Negative ESKAPE GroELs Are Selectively Inhibited by PBZ1587 and Contain a Greater Number of Conserved PBZ1587-Contact Residues Than That of *E. faecium* GroEL.

The extent of PBZ1587-mediated inhibition of ESKAPE GroES/GroEL refolding activity was measured by using the above MDH refolding activity assay to determine if PBZ1587 is active against these chaperones. Although potent inhibition of Gram-negative ESKAPE pathogen GroES/GroEL by PBZ1587 was noted, *E. faecium* (Gram-positive ESKAPE) GroES/GroEL PBZ1587-mediated inhibition was notably weaker (Figure 4A). Prompted by the striking difference between the ESKAPE pathogen Gram-negative chaperones and the Gram-positive chaperone biochemical response to PBZ1587, we aligned *E. coli* and ESKAPE GroEL sequences corresponding to the RRI residues uncovered with our *E. coli*-PBZ1587 structure to identify if differences in these amino acids could explain the discrepancy in potency (Figure 4B). *E. coli* GroEL-PBZ1587 contact residues were found to be more conserved in Gram-negative ESKAPE GroELs than in Gram-positive ESKAPE GroELs. Residue differences for *P. aeruginosa* GroEL (Gram-negative ESKAPE pathogen with the lowest overall amino acid identity compared to *E. coli* GroEL) and *E. faecium* GroEL were compared to the PBZ1587 *E. coli* GroEL binding site residues. The only difference in the PBZ1587-binding region in *E. coli* compared to that in *P. aeruginosa* GroEL is the replacement of V422 with a leucine at the same position. We note that V442L *E. coli* GroEL mutants are potently inhibited by PBZ1587, which would explain why *P. aeruginosa* GroEL is inhibited to a similar extent as *E. coli* GroEL (Figures 3 and 4A,B). All other Gram-negative ESKAPE pathogen GroELs are inhibited potently by PBZ1587, and amino acid alignment of the PBZ1587-binding region supports the similarity of the binding sites for these various GroEL chaperones (Figure 4B). For *E. faecium* GroEL, nearly half of the residues at the *E. coli* GroEL-PBZ1587 binding site are different but retain similar characteristics (M111 is replaced by alanine in *E. faecium*, V438 is replaced by threonine in *E. faecium*, and V442 is replaced by isoleucine in *E. faecium*) (Figure 4B). Revealed by modeling was *E. coli* GroEL V442L with PBZ1587 at the RRI (Figure 4C). Conversely, PBZ1587 was not found at the RRI (or any other site) when incubated with *E. faecium* GroEL (Figure 4D). These data suggest that the PBZ molecules discussed (PBZ1587 and 1038) would not be expected to have broad-spectrum antibacterial activity. However, the data also

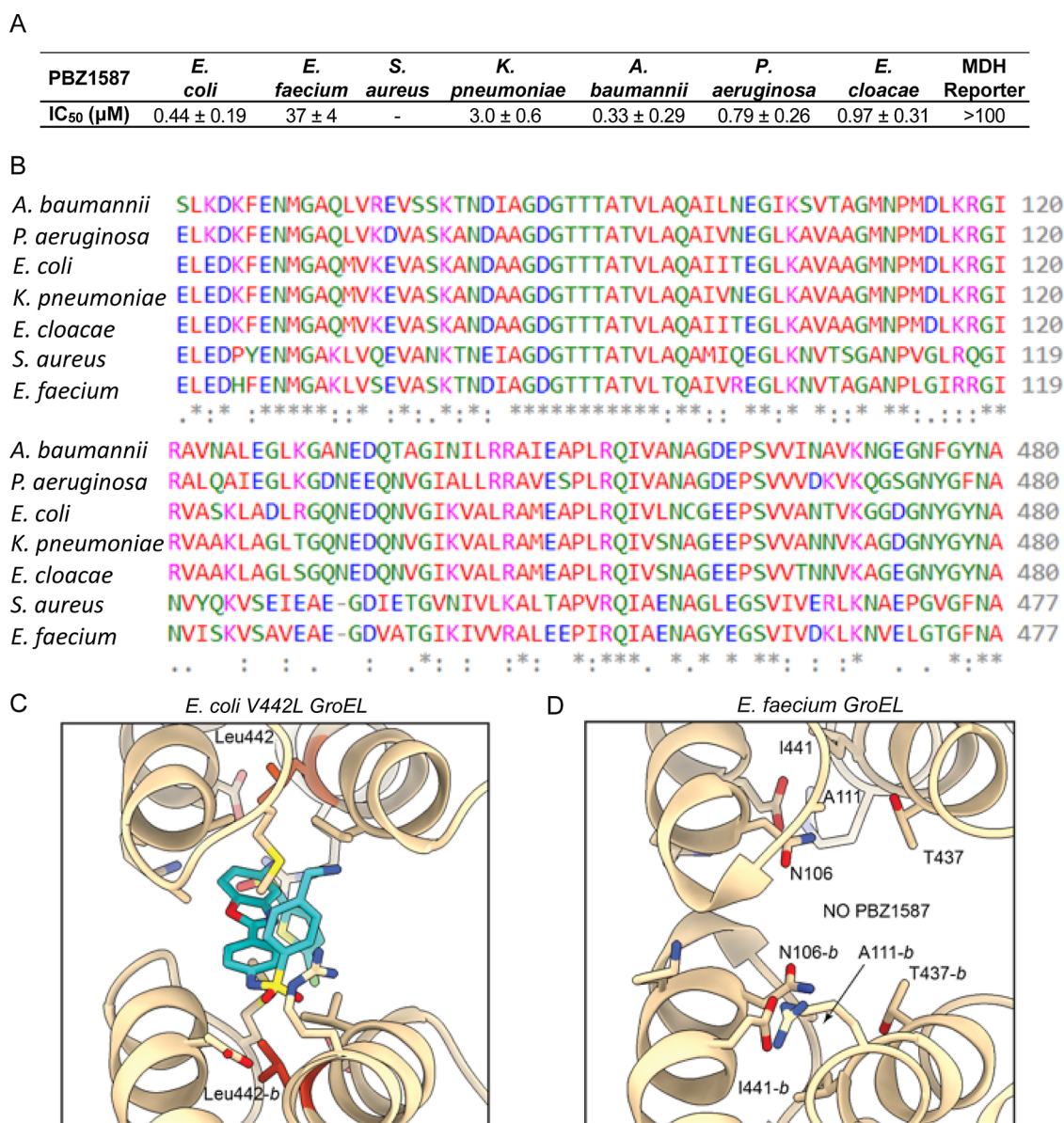


Figure 4. *E. coli* and Gram-negative ESKAPE GroELs are selectively inhibited by PBZ1587 and contain a greater number of conserved PBZ1587-contact residues than that of *E. faecium* GroEL. (A) IC₅₀ values for PBZ1587-mediated inhibition of *E. coli* and ESKAPE GroEL MDH refolding activity. Respective GroES from each strain were used in the assay. *S. aureus* GroES/GroEL could not be expressed/purified (untested). IC₅₀ values for data were obtained in triplicate using a 3-fold dilution series from 0.1 mM to 1.7 nM, and the error was expressed as SEM. (B) Clustal Omega (EMBL-EBI) multiple sequence amino acid alignment between ESKAPE and *E. coli* GroELs. Potential PBZ1587-*E. coli* GroEL contact residues from our cryo-EM structure (Figure 2) and the corresponding ESKAPE GroEL-aligned residues are outlined in black. *S. aureus* and *E. faecium* are Gram-positive, and all others are Gram-negative bacteria. (C) Closeup view of the PBZ1587 binding site at the RRI for modeled *P. aeruginosa* GroEL from the *E. coli* GroEL cryoEM structure with the L442 V mutation (shown in red). Only Leu442 is different from *E. coli* GroEL in this region. (D) Closeup view of RRI for *E. faecium* GroEL from the cryoEM structure (PDB ID 9C0D), highlighting several amino acid substitutions different from *E. coli* GroEL in this region. Residue numbers are shifted due to a 1-residue deletion of N433 in Gram-positive GroEL. *E. faecium* T437 aligns with V438 in *E. coli* GroEL, and *E. faecium* I441 aligns with V442 in *E. coli* GroEL.

provide a structural basis to synthesize PBZ derivatives that would be effective against Gram-positive bacteria. Adjacent residues (with the exception of A106 later discussed) were not investigated to determine what impact, if any, they may have on the orientation of the six potential interacting residues in question and how this may have modulated drug affinity at this site.

***E. faecium* GroEL Residue N106 May Sterically Hinder PBZ1587-GroEL Binding.** In addition to the residues forming interactions with PBZ1587, a key difference in the

proposed PBZ1587-binding site for *E. coli* and *E. faecium* GroEL is pocket size, dictated by residue 106 (alanine vs asparagine, respectively) (Figures 4 and 5A,B). We hypothesized that the less bulky A106 residue allows PBZ1587 entry and residence within the *E. coli* RRI. Conversely, when the *E. faecium* GroEL structure was overlaid onto that of *E. coli* GroEL, N106 appeared to sterically hinder or obstruct molecule binding in the pocket (Figure 5C). GroEL residue 106 mutants were made to explore whether modification of this residue could sensitize *E. faecium* GroEL (N106A) or

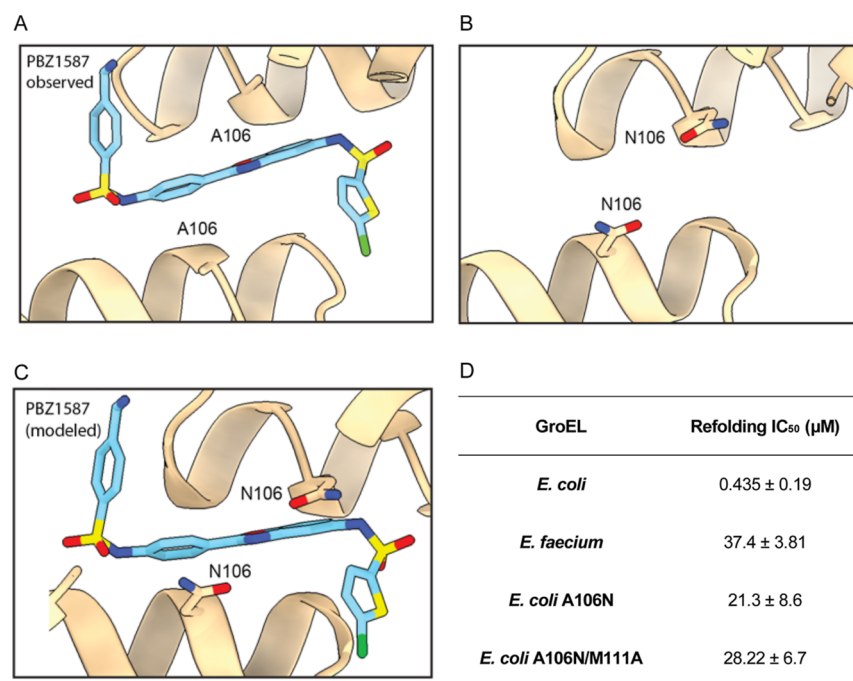


Figure 5. *E. faecium* GroEL residue N106 may sterically hinder PBZ1587-GroEL binding. (A) *E. coli* GroEL RRI highlighting alanine106 as an accommodating residue of PBZ1587 from the cryoEM structure (PDB ID 9C0B). (B) Modeled *E. faecium* GroEL RRI from the cryoEM structure (PDB ID 9C0C), highlighting asparagine106 acting to sterically hinder PBZ1587 binding. (C) Superimposition of PBZ1587 from *E. coli* docked with GroEL from *E. faecium* (PDB ID 9C0D), highlighting steric incompatibility (1.5 Å distance between N106 and PBZ1587). (D) PBZ1587-mediated inhibition of refolding activity for *E. coli*, *E. faecium*, and mutant GroELs. WT *E. coli* GroES was included in each refolding experiment. IC₅₀ values for data were obtained in triplicate with a 3-fold dilution series from 0.1 mM to 1.7 nM, and the error was expressed as SEM.

make *E. coli* GroEL (A106N) resistant to PBZ1587. *E. coli* A106N and A106N/M111A (the bulkiness of the asparagine mutant was initially predicted to clash with M111, and thus, the A106N/M111A mutant was made to compensate for steric hindrance) were expressed and purified for biochemical analysis. We were surprised to find that M111A was now tolerated when coupled with the A106N mutation. Unfortunately, *E. faecium* N106A and N106A/A111 M GroEL mutations were lethal to the organism when expressed (dominant negative effects) and could not be studied. *E. coli* A106N and A106N/M111A GroEL mutants retained refolding activity (Figure S2). *E. coli* A106N and A106N/M111A GroEL were more resistant to PBZ1587-mediated inhibition in the client-refolding reporter assay, in line with *E. faecium* GroEL biochemical observations (Figure 5D). Barring other variables, differential PBZ1587 engagement among ESKAPE GroES/GroEL chaperone systems may explain the variance in sensitivity to PBZ1587 in ESKAPE pathogens.

PBZ1587 Engages GroEL in the Cell but Shows Off-Target Effects, Whereas GroEL Targeting Is Likely the Primary Mode of PBZ1038 Action. To support on-target activity in bacteria, a reporter system utilizing mutated eGFP (D117/G116) was employed (previously developed by the Horovitz group^{32,33}). This fluorescent reporter remains unfolded after translation and can be folded to its native fluorescent state only by the GroES/GroEL chaperone system. We employed *acrB* knockout (Δ *acrB*) (multidrug efflux pump deficient) *E. coli* cells^{34,35} expressing either *E. coli* GroES/GroEL or *E. faecium* GroES/GroEL with a plasmid expressing D117/G116 eGFP and monitored fluorescence signal in the presence of increasing doses of PBZ1587 (Figure 6A). In the presence of the *E. faecium* GroES/GroEL, the EC₅₀ was shifted

approximately 4-fold, arguing that PBZ1587 engages GroEL in the cells (Figure 6A,E). To test if GroEL was responsible for the PBZ1587 cellular mode of action, Δ *acrB* *E. coli* expressing *E. coli* GroES/GroEL or Δ *acrB* *E. coli* expressing *E. faecium* GroES/GroEL were treated with increasing doses of PBZ1587; however, there was no significant shift in the observed CC₅₀ in the presence of *E. faecium* GroES/GroEL (Figure 6B,E). Despite engaging GroEL (Figure 6A), the lack of a shift in CC₅₀ argued that PBZ1587 had off-target effects in the cells. Because of the putative off-target effects of PBZ1587, we next examined a related PBZ analogue, PBZ1038, with parphenolic end-capping groups (Figure 7B). Of all our PBZ series analogues, PBZ1038 is the most potent at inhibiting GroEL ATPase and client protein-folding functions. We first measured the PBZ1038 effects in the eGFP reporter strain and observed a 5-fold increase in EC₅₀ in the presence of *E. faecium* GroES/GroEL relative to *E. coli* GroES/GroEL (Figure 6C,E), indicating GroEL engagement in the cells. To test if GroEL inhibition was responsible for the antibacterial activity, we used the Δ *acrB* *E. coli* expressing *E. coli* GroES/GroEL or the Δ *acrB* *E. coli* expressing *E. faecium* GroES/GroEL and observed an 8-fold shift in CC₅₀ values for PBZ1038 (Figure 6D,E). These data argued that GroEL was the target, leading to the observed activity.

PBZ1038 Binds the RRI and Shows Decreased Activity against *E. faecium* GroES/GroEL Refolding of MDH. To determine if PBZ1038 bound in a manner similar to that of PBZ1587, we first used AutoDock to predict the binding site and pose of PBZ1038 (Figure 7B), which showed PBZ1038 bound to the RRI at the same position as PBZ1587 and assumed a similar orientation (Figure 7A). Our initial attempts to get PBZ-GroEL costructures by cryoEM used

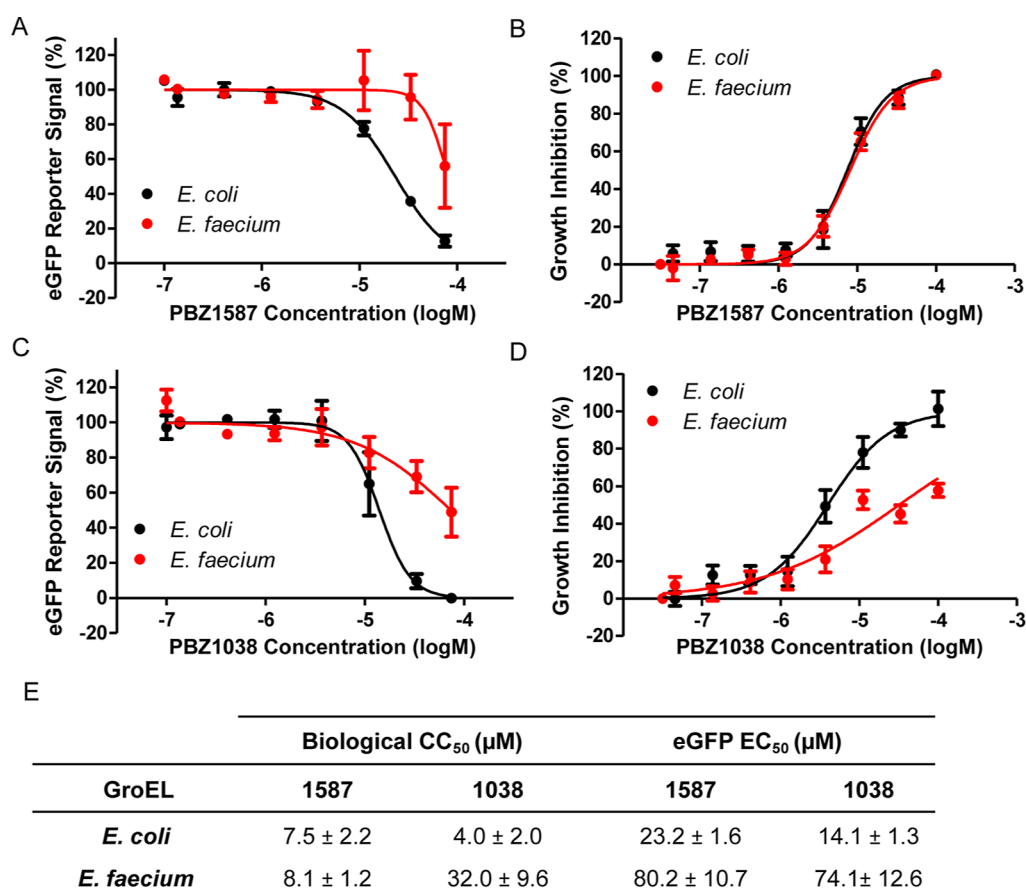


Figure 6. PBZ1587 engages GroEL in the cell but shows off-target effects, whereas GroEL targeting is likely the primary mode of PBZ1038 action. (A) MG1655 Δ acrB *E. coli* expressing the D117/G116 eGFP reporter and either *E. coli* GroES/EL or *E. faecium* GroES/EL in the chromosome treated with PBZ 1587. Values for OD₆₀₀ and the fluorescent signal were normalized to DMSO-treated cells, and then each fluorescent signal was normalized to the final OD₆₀₀. (B) PBZ1587 dose response in MG1655 Δ acrB *E. coli* with a chromosomal copy of *E. coli* GroES/EL or in MG1655 Δ acrB *E. coli* with a chromosomal copy of *E. faecium* GroES/EL replacing the endogenous copy. (C) eGFP reporter in strains from A with PBZ1038. (D) PBZ1038 dose response in the same strains as B. (E) Tabulated CC₅₀ and IC₅₀ values from A to D. Experiments were completed in at least triplicate with a 3-fold dilution series from 0.1 mM to 1.7 nM, and the error was expressed as SEM.

PBZ1038; however, we observed a large amount of precipitation upon addition of the compound and observed no compound occupancy in the structures. We assumed this was due to compound solubility as PBZ1587 is much more soluble than PBZ1038. As anticipated, PBZ1038 also showed a large shift when tested against *E. faecium* GroES/GroEL-mediated MDH refolding with no effects on native MDH (Figure 7C), further confirming similar binding to that for PBZ1587. Finally, using the GroEL mutants reported in Figures 3 and 5, we tested the effects of these RRI mutants on the PBZ1038 inhibition of GroES/GroEL-mediated MDH refolding (Figure 7D). In each case, we saw shifts like those for PBZ1587, including increased potency in the case of the V442L mutant (Figure 7D,E). Collectively, these data support the notion that PBZ1038 binds to GroEL in the same position as PBZ1587 and has a similar mechanism of inhibition.

Expression of GroEL Mutants Rescues PBZ1038 Cellular Toxicity in Δ acrB *E. coli*. As a further confirmation of GroEL inhibition being the driver of antibacterial effects, we expressed three of the mutants that showed the largest IC₅₀ shifts in the MDH-refolding assay in the *E. coli* strain MC4100. In the presence of PBZ1587, we observed no shift in CC₅₀ (data not shown). However, in the presence of PBZ1038, the V438A mutant showed an approximately 8-fold shift in CC₅₀, and the A106N and A106N/M111A mutants showed >20-fold

shifts in CC₅₀ (Figure 8A,B, S3A,B, S4A,B, and S5A,B). We also observed that these CC₅₀ shifts correlate with the level of expression of the given mutants (uninduced vs induced in Figures S3–S5). Collectively, these data argue for GroEL inhibition as the primary mode of antibacterial action.

CONCLUSIONS

Cryo-EM, molecular modeling, and mutagenesis studies uncovered the GroEL RRI as the binding site of two of our lead chaperone inhibitors, PBZ1587 and PBZ1038. Both PBZ compounds were found to potently inhibit the refolding activity of *E. coli* and the Gram-negative ESKAPE pathogen GroES/GroEL but not the Gram-positive ESKAPE pathogen *E. faecium* GroES/GroEL. Biochemical inhibition of *E. coli* GroES/GroEL refolding activity was more sensitive to the PBZ compounds than *E. faecium* GroES/GroEL. However, despite a shift in the inhibition of eGFP in a cellular reporter assay (23.2 vs 80.2 μM), PBZ1587 failed to show a statistically significant shift in CC₅₀ when *E. faecium* was the only copy of GroES/GroEL in *E. coli* cells. There was also no shift in CC₅₀ when PBZ1587-resistant mutants were expressed in *E. coli* cells (data not shown). However, PBZ1038 showed a robust shift in CC₅₀ in the presence of *E. faecium* chaperonin and a shift in EC₅₀ in the eGFP reporter assay in the presence of *E. faecium*

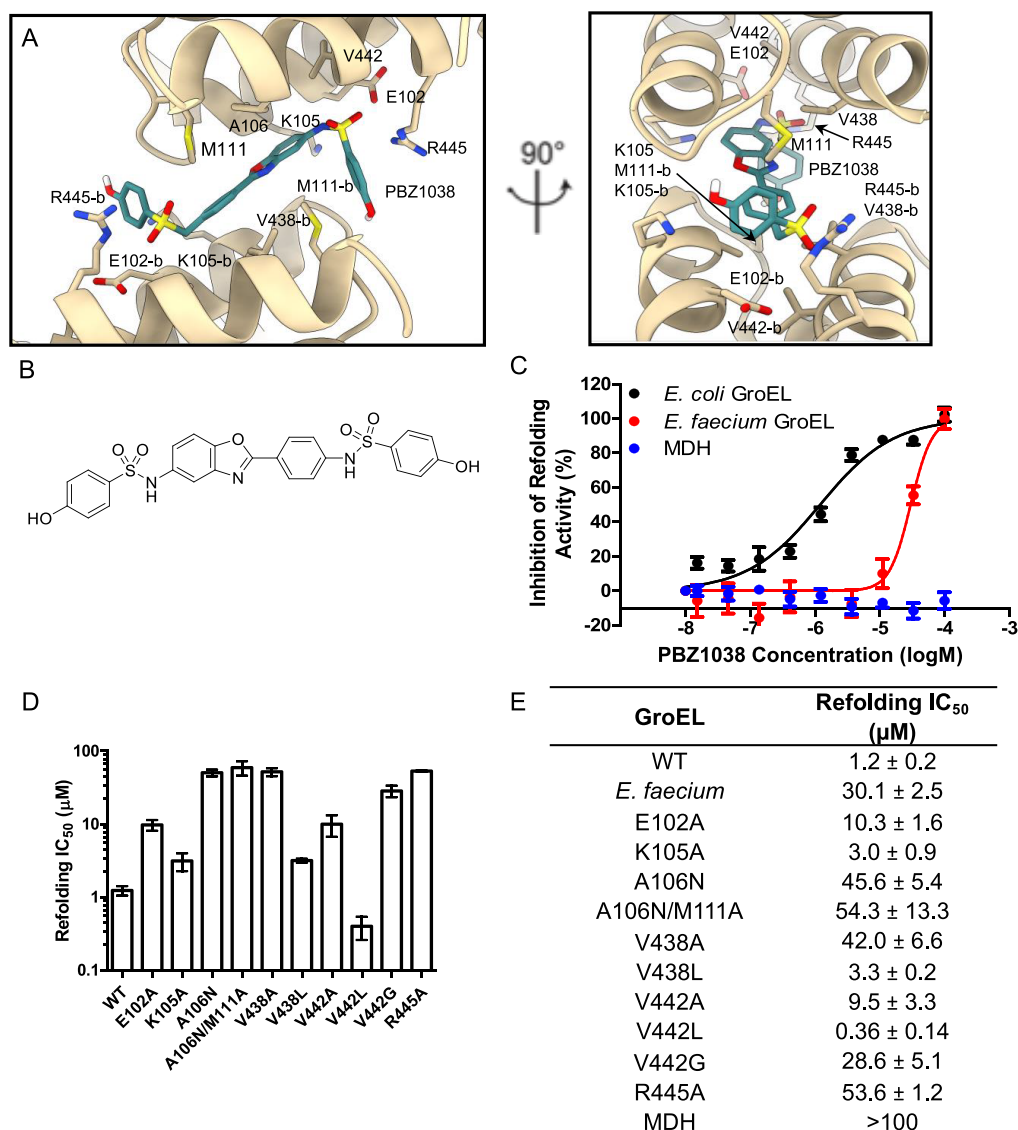


Figure 7. PBZ1038 binds the RRI and shows decreased activity against *E. faecium* GroES/GroEL refolding of MDH. (A) PBZ1038 docked onto *E. coli* GroEL (PDB ID 9C0B) with contact residues labeled. (B) Structure of PBZ1038. (C) PBZ1038-mediated inhibition of refolding activity for *E. coli* GroES/EL (black), *E. faecium* GroES/EL (red), or native MDH (blue). (D) PBZ1038-mediated inhibition of the refolding activity of WT and mutant GroELs. (E) Tabulated values from C and D. Experiments were completed in triplicate with a 3-fold dilution series from 0.1 mM to 1.7 nM, and the error was expressed as SEM.

chaperonin. Furthermore, the recalcitrant RRI mutants were able to rescue *E. coli* cells when expressed off of plasmids in the presence of PBZ1038. To our knowledge, this is the first report of a small-molecule exerting antimicrobial effects established through on-target-mediated inhibition of cellular GroEL activity. Future work will include modifying the current PBZ1038 scaffold to improve penetration and accumulation of Gram-negative pathogens using the eNTRY rules.^{36,37}

EXPERIMENTAL SECTION

Preparation of Samples for Cryo-Electron Microscopy.

Purified complexes of 6 mg/mL *E. coli* GroEL and 7.1 mg/mL *E. faecium* GroEL were prepared without PBZ1587 or in the presence of a 20-fold molar excess of the PBZ1587 ligand in buffer comprising 50 mM Tris pH 7.5, 150 mM NaCl, 2 mM TCEP, and <1% dimethyl sulfoxide (DMSO). Complexes treated with a ligand were incubated for 5 min at 4 °C prior to plunging. Quantifoil 300 mesh R1.2/1.3 UltrAuFoil Holey gold films were glow discharged for 25 s with Pelco Easiglow 91000 (Ted Pella, Inc.) in ambient vacuum. Four μL of the

sample was applied and blot-plunged using a manual plunge freezer in a 4 °C cold room with >95% humidity. Grids were blotted for ~3 s and immediately plunged into a liquid ethane pool cooled by liquid nitrogen.

Cryo-EM Data Acquisition. Cryo-EM data were collected on a Thermo-Fisher Talos Arctica transmission electron microscope operating at 200 keV using parallel illumination conditions.³⁸ Micrographs were acquired using a Gatan K2 Summit direct electron detector, operated in electron counting mode, with a total electron exposure of 54 e⁻/Å². The Legicon data collection software³⁹ was used to collect micrographs at 36,000× nominal magnification (1.15 Å/pixel at the specimen level) with a nominal defocus set to 0.8–1.2 μm under focus. Stage movement was used to target the center of four 1.2 μm holes for focusing, and an image shift was used to acquire high-magnification images in the center of each of the four targeted holes. 1013 micrographs were collected at 1.15 Å pixel for liganded *E. coli*, 276 for apo *E. coli*, 287 for liganded *E. faecium*, and 341 for apo *E. faecium* complexes.

Cryo-EM Image Analysis. Cryo-EM movies were transferred to Warp v1.0.9⁴⁰ for motion correction, CTF correction, and particle

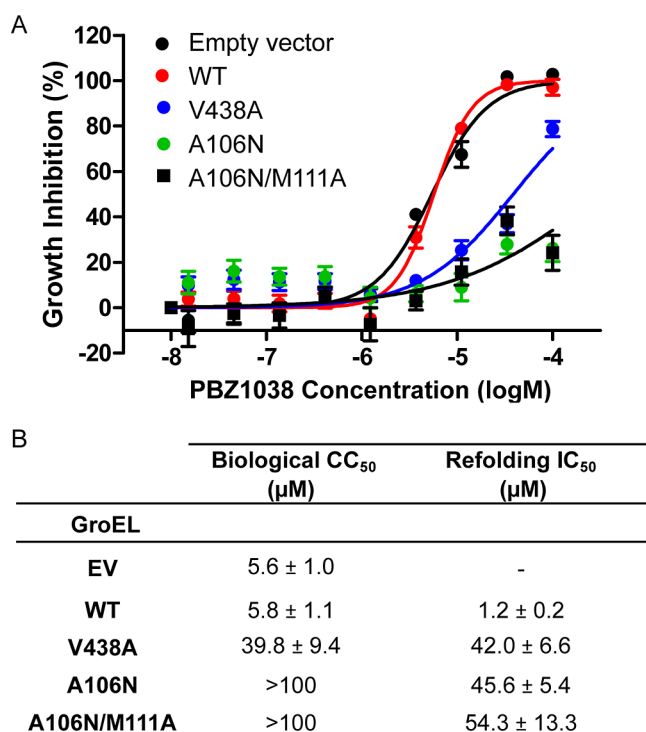


Figure 8. Expression of GroEL mutants rescues PBZ1038 cellular toxicity in Δ *acrB* *E. coli*. (A) PBZ1038 dose response in MC4100 Δ *acrB* *E. coli* expressing an empty vector (black circles), wild-type GroEL (red circles), V438A GroEL (blue circles), A106N GroEL (green circles), or A106N/M111A GroEL (black squares). (B) Tabulated CC₅₀ values for MC4100 Δ *acrB* *E. coli* expressing the indicated GroEL mutants and IC₅₀ values for dMDH refolding. Experiments were completed in triplicate using a 3-fold dilution series from 0.1 mM to 1.7 nM, and errors were expressed as SEM.

picking, 26,066 particles, 12,714 particles, 4621 particles, and 13,898 particles were picked for liganded *E. coli*, apo *E. coli*, liganded *E. faecium*, and apo *E. faecium* complexes, respectively. Particles were extracted with a 256 pixel box size and imported to cryoSPARC v3.3.2⁴¹ for cleanup based on two-dimensional classification and all subsequent processing steps. Initial models were generated ab initio from selected particles and used to seed homogeneous or NU-refinement of all-quality particles. Per-particle defocus and up to fourth-order optical aberrations were corrected in cryoSPARC's NU-refinement protocol, and symmetry was automatically applied at this step when noted. After visualization that all *E. faecium* particles were apo, they were pooled and refined together to generate the final apo map.

Atomic Model Building and Refinement. Model building and refinement were initiated with published models for *E. coli* GroEL. Restraints and the original PDB for PBZ1587 were generated with the GRADE server.⁴² Iterative rounds of model building and refinement were performed in PHENIX v1.19.2⁴³ and Coot 0.9-pre EL revision 8983⁴⁴ until reasonable agreement between the model and data was achieved. UCSF Chimera and ChimeraX⁴⁵ were used to interpret the EM reconstructions and atomic models, as well as to generate figures.

Bacterial Strains and Plasmids. The bacterial strain used for expression of WT *E. coli* GroES/GroEL and mutant *E. coli* GroEL was T7 Express *E. coli* (cam^R) (NEB).

E. faecium GroESL was expressed in an MG1655 knock-in strain²⁷ (containing chromosomal *E. faecium* *groESL* (cam^R), which replaced *E. coli* *groESL*) using *E. faecium* *groESL* cloned into pET21b (amp^R) along with pCS6 (T7 RNA polymerase helper plasmid, spec^R)⁴⁶ for overexpression (single copy, chromosomal expression yields much lower protein than plasmid overexpression). A similar procedure was used for *P. aeruginosa* GroESL using an MG1655 knock-in strain

containing chromosomal *P. aeruginosa* *groESL* (cam^R), which replaced *E. coli* *groESL*.

Cell viability assays were performed in *acrB* knockout *E. coli* (kan^R).^{34,35} *acrB* knockout *E. coli* (kan^R) containing *E. faecium* *groESL* [chromosomal *E. faecium* *groESL* (cam^R), which replaced *E. coli* *groESL*] was generated by P1 phage transduction⁴⁷ using the MG1655 knock-in strain containing *E. faecium* *groESL* as above.

The D117/G116 eGFP plasmid (pET28a, T7-promoted, kan^R) was provided by the Amnon Horovitz group^{32,33} for overexpression in *E. coli* and was subsequently subcloned into pET21b (T7-promoted, amp^R).

The *Trc*-promoted *E. coli* GroES/GroEL plasmid (amp^R) was used for overexpression. GroEL mutants were generated using this parent plasmid by the Naismith method.⁴⁸

Protein Expression and Purification. The *Trc*-promoted *E. coli* GroES/GroEL plasmid (amp^R) was transformed into T7 Express *E. coli* (cam^R) with overnight positive selection on 0.1 mg/mL ampicillin and 0.025 mg/mL chloramphenicol LB agar plates. Single colonies were picked and grown overnight in LB media (shaking at 250 rpm, 37 °C) and then diluted 1:25 in 250–500 mL of terrific broth (2 L baffled flask) containing 0.1 mg/mL ampicillin. OD₆₀₀ was monitored, and protein expression was induced at an OD₆₀₀ of 0.8 with 1 mM IPTG. Expression was allowed to continue for up to 4 h at 37 °C, after which cells were pelleted at 7200 g for 10 min at 4 °C. Pellets were resuspended in 50 mM Tris pH 7.4, 50 mM KCl, 1 mM DTT, and 1 mM PMSF and homogenized using Microfluidizer LM10. The lysate was clarified by centrifugation (22,000g for 45 min) at 4 °C. The clarified lysate was loaded onto pre-equilibrated FFQ resin (Cytiva) and eluted using a 0 to 1 M NaCl (containing 50 mM Tris pH 7.4, 1 mM DTT buffer) gradient over 10 column volumes. GroEL-containing fractions were pooled, stirred, and slowly adjusted to 1.2 M ammonium sulfate at 4 °C, followed by clarification at 4 °C for 45 min at 22,000g. The clarified pool was added to a pre-equilibrated source 1SISO (Cytiva) and eluted over 1 column volume with 50 mM Tris pH 7.4, 50 mM KCl, 150 mM NaCl, and 1 mM DTT. Pooled GroEL fractions were dialyzed against buffer containing 50 mM Tris pH 7.4, 150 mM NaCl, and 1 mM DTT and then stored at 4 °C or flash-frozen for future use.

T7-promoted *E. faecium* *groESL* (pET21b, amp^R) along with *P*_{BAD}-promoted pCS6 (T7 RNA polymerase helper plasmid, spec^R) were transformed into MG1655 knock-in bacteria (cam^R) (containing chromosomal *E. faecium* *groESL*, which replaced *E. coli* *groESL*) with overnight positive selection on 0.1 mg/mL ampicillin, 0.05 mg/mL spectinomycin, and 0.025 mg/mL chloramphenicol. All expression steps from above were identical, with the exception of induction with 0.2% arabinose. The *E. faecium* GroEL purification was performed as described above.

E. coli and *E. faecium* GroES were expressed as described above, with the following exceptions: GroES was loaded onto preequilibrated FFQ resin (Cytiva) and eluted using a 0 to 1 M NaCl (containing 50 mM Tris pH 7.4, 1 mM DTT buffer) gradient over 10 column volumes. GroES-containing fractions were pooled and adjusted to pH 4.6 using 50 mM sodium acetate pH 4.6 buffer. pH-adjusted GroES was added to a preequilibrated FFSP (Cytiva) column and eluted over 10 column volumes using a 0 to 1 M NaCl (containing 50 mM Tris pH 4.6, 1 mM DTT buffer) gradient. GroES-containing fractions were pooled, concentrated, and loaded onto a preequilibrated Hiload 26/600 Superdex 75 (GE) and eluted in less than one column volume in buffer containing 50 mM Tris pH 7.4, 300 mM NaCl, and 1 mM DTT buffer. GroES fractions were analyzed by SDS-PAGE for purity, as well as by native PAGE and/or electron microscopy (in concert with GroEL) for proper quaternary structure. Pooled fractions were concentrated and stored at 4 °C or frozen for future use.

***E. coli* Growth Inhibition Assay.** In LB media, *acrB* knockout cells (kan^R)^{34,35} were grown overnight shaking (250 rpm) at 37 °C with positive antibiotic selection (0.05 mg/mL kanamycin). In the morning, cells were diluted 1:5 in fresh LB medium (without antibiotics) and grown for 2 h with continued shaking as above. After 2 h, cells were diluted to an OD₆₀₀ of 0.0125 with fresh LB media (without antibiotics) and incubated with PBZ1587 or PBZ1038 (3-

fold dilution series from 0.1 mM to 1.7 nM final concentration) or DMSO and added to a 384-well plate at a volume of 0.1 mL. Plates were then covered with an oxygen-permeable membrane (Breathe-Easy, Diversified Biotech) and incubated in a stationary 37 °C incubator for 24 h. Plates were read using a SpectraMax ID5 plate reader at 600 nm absorbance at the end time point.

D117/G116 eGFP Assay. The T7-promoted D117/G116 eGFP plasmid^{32,33} (pET21b, amp^R) was transformed into *acrB* knockout *E. coli* (kan^R) or *acrB* knockout *E. coli* (kan^R) with *E. faecium* *groESL* (cam^R) replacing *E. coli* *groESL* and underwent positive antibiotic selection overnight on LB agar plates. Colonies were next grown overnight with positive antibiotic selection in LB medium and diluted 1:5 with fresh LB medium (without antibiotics). A maximum of 1 mL of each culture (in a 15 mL culture tube) was grown to an OD₆₀₀ of 0.6 and induced with 1 mM IPTG after incubating with PBZ1587 or PBZ1038 for 15 min. 0.15 mL from each sample was removed after 90 min and centrifuged at 5000g for 5 min. After centrifugation, the supernatant was discarded, and cells were resuspended in 0.15 mL of M9 media and then plated into a 96-well plate (black plate, clear bottom, Corning costar 3603). OD₆₀₀ and eGFP fluorescence (475 nm excitation/515 nm emission) were obtained using a SpectraMax ID5 plate reader. Data were generated in at least triplicate, with averages plotted using GraphPad Prism 6.0.

Refolding Assay. Refolding of denatured MDH (dMDH) by the ESKAPE GroES/GroEL chaperonin systems was performed as previously reported with *E. coli* GroESL.¹⁴ Five mg/mL MDH from porcine heart (Sigma) was diluted 1:1 with denaturation solution (7 M guanidine, 50 mM Tris pH 7.4, 50 mM DTT) for 1 to 3 h at room temperature before forming a binary complex (83.3 nM GroEL and 20 nM dMDH) in 50 mM Tris pH 7.4, 50 mM KCl, 10 mM MgCl₂, 1 mM DTT, and 0.1% Tween 20 (the final guanidine concentration is less than 1 mM and does not significantly alter chaperonin function). GroES was added (100 nM final concentration) to the binary solutions, and a volume of 30 μL was dispensed into a clear 384-well plate (Greiner). In addition to GroES, GroEL, and dMDH solution (binary solution), three controls were tested to ensure assay reliability: (1) native MDH-only control (to measure the maximum MDH activity rate), (2) dMDH-only control (to measure spontaneous refolding activity), and (3) GroEL and dMDH only (to measure the ability of GroEL to trap and hold dMDH without GroES-assisted refolding). To each of the four solutions, 20 μL of ATP solution (in binary buffer) at a concentration of 2.5 mM was added to start the refolding process. The assay was incubated at 37 °C and quenched with 10 μL of 0.6 M EDTA pH 8.0 at multiple time points (for determination of refolding kinetics). To determine the extent of dMDH refolded, 20 μL of assay solution (50 mM Tris pH 7.4, 50 mM KCl, 1 mM DTT, 0.1% Tween 20, 20 mM sodium mesoxalate, and 2.4 mM NADH) was added to all wells, followed by monitoring absorbance values at 340 nm using a SpectraMax ID5 plate reader. The procedure (single time point exception) was also used to determine the extent of refolding inhibition with PBZ1587 or PBZ1038 by incubating each solution with PBZ1587 or PBZ1038 at the appropriate concentration (3-fold dilution series from 0.1 mM to 1.7 nM) before the binary complex was formed. Absorbance readings were taken every 5 min until absorbance values reached their minima. Rate determination and figure generation were done by plotting data in GraphPad Prism 6.0. All data were generated at least in triplicate.

AutoDock Simulations. Molecules of PBZ (1587, 1038) were prepared in ChemDraw Version 22.2 (PerkinElmer). Schrödinger Maestro version 13.7 was selected for ligand conformational search, and docking was performed using our solved Cryo-EM structure of *E. coli* GroEL. Each molecule was docked, and the minimum energy outputs for each interaction are displayed. Figures for each model were created by using UCSF ChimeraX.

■ ASSOCIATED CONTENT

Data Availability Statement

All cryoEM data reported are available through the RCSB PDB (<https://www.rcsb.org/>). PDB IDs: 9C0C—apo *E. coli*

GroEL; 9C0B—PBZ1587 liganded *E. coli* GroEL; and 9C0D—*E. faecium* GroEL. EMDB IDs: EMD-45079—apo *E. coli* GroEL; EMD-45078—PBZ1587 liganded *E. coli* GroEL; and EMD-45080—*E. faecium* GroEL.

Supporting Information

The Supporting Information is available free of charge at <https://pubs.acs.org/doi/10.1021/jacs.4c05057>.

CryoEM data collection; CryoEM refinement statistics; PBZ1587 bound to seven GroEL pockets; GroEL amino acids interacting with PBZ1587; GroEL trapping and refolding of dMDH; GroEL-V438A rescuing cytotoxicity of PBZ1038; GroEL-A106N rescuing cytotoxicity of PBZ1038; and GroEL-A106N/M111A rescuing cytotoxicity of PBZ1038 (PDF)

■ AUTHOR INFORMATION

Corresponding Authors

Gabriel C. Lander – Department of Integrative Structural and Computational Biology, Scripps Research, La Jolla, California 92037, United States; Phone: 858-784-8793;

Email: glander@scripps.edu

Eli Chapman – College of Medicine, Department of Pharmacology and Therapeutics, Center for Inflammation Science and Systems Medicine, The Herbert Wertheim UF Scripps Institute for Biomedical Innovation and Technology, University of Florida, Jupiter, Florida 33458, United States; orcid.org/0000-0002-6310-1664; Phone: 561-228-2559; Email: chapmaneli@ufl.edu

Authors

Jack Godek – College of Medicine, Department of Pharmacology and Therapeutics, Center for Inflammation Science and Systems Medicine, The Herbert Wertheim UF Scripps Institute for Biomedical Innovation and Technology, University of Florida, Jupiter, Florida 33458, United States

Jared Sivinski – College of Pharmacy, Department of Pharmacology and Toxicology, The University of Arizona, Tucson, Arizona 85721, United States

Edmond R. Watson – Department of Integrative Structural and Computational Biology, Scripps Research, La Jolla, California 92037, United States

Felicidad Lebario – College of Medicine, Department of Pharmacology and Therapeutics, Center for Inflammation Science and Systems Medicine, The Herbert Wertheim UF Scripps Institute for Biomedical Innovation and Technology, University of Florida, Jupiter, Florida 33458, United States

Wenli Xu – College of Pharmacy, Department of Pharmacology and Toxicology, The University of Arizona, Tucson, Arizona 85721, United States

Mckayla Stevens – Department of Biochemistry and Molecular Biology, Indiana University School of Medicine, Indianapolis, Indiana 46202, United States

Christopher J. Zerio – College of Pharmacy, Department of Pharmacology and Toxicology, The University of Arizona, Tucson, Arizona 85721, United States

Andrew J. Ambrose – College of Pharmacy, Department of Pharmacology and Toxicology, The University of Arizona, Tucson, Arizona 85721, United States; orcid.org/0000-0002-2932-4514

Xiaoyi Zhu – College of Medicine, Department of Pharmacology and Therapeutics, Center for Inflammation Science and Systems Medicine, The Herbert Wertheim UF

Scripps Institute for Biomedical Innovation and Technology,
University of Florida, Jupiter, Florida 33458, United States;
orcid.org/0000-0002-2049-9561

Carlee A. Trindl – College of Medicine, Department of
Pharmacology and Therapeutics, Center for Inflammation
Science and Systems Medicine, The Herbert Wertheim UF
Scripps Institute for Biomedical Innovation and Technology,
University of Florida, Jupiter, Florida 33458, United States

Donna D. Zhang – The Herbert Wertheim UF Scripps
Institute for Biomedical Innovation and Technology, Center
for Inflammation Science and Systems Medicine, Jupiter,
Florida 33458, United States

Steven M. Johnson – Department of Biochemistry and
Molecular Biology, Indiana University School of Medicine,
Indianapolis, Indiana 46202, United States; orcid.org/
0000-0001-7254-4128

Complete contact information is available at:
<https://pubs.acs.org/10.1021/jacs.4c05057>

Author Contributions

[#]J.G., J.S., and E.R.W. contributed equally.

Notes

The authors declare the following competing financial interest(s): S.M.J. and E.C. are cofounders of BioEL, Inc.

ACKNOWLEDGMENTS

We would like to thank Arthur Horwich for supplying the *E. coli* strain LG6 and Amnon Horowitz for providing the D117/G116 eGFP plasmid. This research was supported by the National Institutes of Health grants R01 GM120350 to E.C. and S.M.J. and R35ES031575 to D.D.Z. and E.C. C.J.Z., J.S., and A.J.A. are funded by T32 GM008804. The content is solely the responsibility of the authors and does not necessarily represent the official views of the NIH.

REFERENCES

- (1) Braig, K.; Otwinowski, Z.; Hegde, R.; Boisvert, D. C.; Joachimiak, A.; Horwich, A. L.; Sigler, P. B. The crystal structure of the bacterial chaperonin GroEL at 2.8 Å. *Nature* **1994**, *371* (6498), 578–586.
- (2) Chapman, E.; Farr, G. W.; Usaite, R.; Furtak, K.; Fenton, W. A.; Chaudhuri, T. K.; Hondorp, E. R.; Matthews, R. G.; Wolf, S. G.; Yates, J. R.; et al. Global aggregation of newly translated proteins in an *Escherichia coli* strain deficient of the chaperonin GroEL. *Proc. Natl. Acad. Sci. U.S.A.* **2006**, *103* (43), 15800–15805.
- (3) Fayet, O.; Ziegelhoffer, T.; Georgopoulos, C. The groES and groEL heat shock gene products of *Escherichia coli* are essential for bacterial growth at all temperatures. *J. Bacteriol.* **1989**, *171* (3), 1379–1385.
- (4) Horovitz, A. The relation between cooperativity in ligand binding and intramolecular cooperativity in allosteric proteins. *Proc. Roy. Soc. Lond. B Biol. Sci.* **1995**, *259*, 85–87.
- (5) Horwich, A. L.; Willison, K. R. Protein folding in the cell: functions of two families of molecular chaperone, hsp 60 and TF55-TCP1. *Philos. Trans. R. Soc. Lond. B Biol. Sci.* **1993**, *339* (1289), 313–325.
- (6) Koshland, D. E.; Nemethy, G.; Filmer, D. Comparison of experimental binding data and theoretical models in proteins containing subunits. *Biochemistry* **1966**, *5* (1), 365–385.
- (7) Monod, J.; Wyman, J.; Changeux, J. P. On the Nature of Allosteric Transitions: A Plausible Model. *J. Mol. Biol.* **1965**, *12*, 88–118.
- (8) Van Dyk, T. K.; Gatenby, A. A.; LaRossa, R. A. Demonstration by genetic suppression of interaction of GroE products with many proteins. *Nature* **1989**, *342* (6248), 451–453.
- (9) Yifrach, O.; Horovitz, A. Two lines of allosteric communication in the oligomeric chaperonin GroEL are revealed by the single mutation Arg196→Ala. *J. Mol. Biol.* **1994**, *243* (3), 397–401.
- (10) Yifrach, O.; Horovitz, A. Nested cooperativity in the ATPase activity of the oligomeric chaperonin GroEL. *Biochemistry* **1995**, *34* (16), 5303–5308.
- (11) Ivic, A.; Olden, D.; Wallington, E.; Lund, P. Deletion of *Escherichia coli* groEL is complemented by a *Rhizobium leguminosarum* groEL homologue at 37°C but not at 43°C. *Gene* **1997**, *194* (1), 1–8.
- (12) Abdeen, S.; Kunkle, T.; Salim, N.; Ray, A. M.; Mammadova, N.; Summers, C.; Stevens, M.; Ambrose, A. J.; Park, Y.; Schultz, P. G.; et al. Sulfonamido-2-arylbenzoxazole GroEL/ES Inhibitors as Potent Antibacterials against Methicillin-Resistant *Staphylococcus aureus* (MRSA). *J. Med. Chem.* **2018**, *61* (16), 7345–7357.
- (13) Abdeen, S.; Salim, N.; Mammadova, N.; Summers, C. M.; Frankson, R.; Ambrose, A. J.; Anderson, G. G.; Schultz, P. G.; Horwich, A. L.; Chapman, E.; et al. GroEL/ES inhibitors as potential antibiotics. *Bioorg. Med. Chem. Lett.* **2016**, *26* (13), 3127–3134.
- (14) Kunkle, T.; Abdeen, S.; Salim, N.; Ray, A. M.; Stevens, M.; Ambrose, A. J.; Victorino, J.; Park, Y.; Hoang, Q. Q.; Chapman, E.; et al. Hydroxybiphenylamide GroEL/ES Inhibitors Are Potent Antibacterials against Planktonic and Biofilm Forms of *Staphylococcus aureus*. *J. Med. Chem.* **2018**, *61* (23), 10651–10664.
- (15) Clatworthy, A. E.; Pierson, E.; Hung, D. T. Targeting virulence: a new paradigm for antimicrobial therapy. *Nat. Chem. Biol.* **2007**, *3* (9), 541–548.
- (16) Santajit, S.; Indrawattana, N. Mechanisms of Antimicrobial Resistance in ESKAPE Pathogens. *BioMed Res. Int.* **2016**, *2016*, 1–8.
- (17) Diekema, D. J.; Pfaller, M. A.; Shortridge, D.; Zervos, M.; Jones, R. N. Twenty-Year Trends in Antimicrobial Susceptibilities Among *Staphylococcus aureus* From the CENTRY Antimicrobial Surveillance Program. *Open Forum Infect. Dis.* **2019**, *6* (Supplement_1), S47–S53.
- (18) Kurosu, M.; Siricilla, S.; Mitachi, K. Advances in MRSA drug discovery: where are we and where do we need to be? *Expert Opin. Drug Discovery* **2013**, *8* (9), 1095–1116.
- (19) Rodvold, K. A.; McConeghy, K. W. Methicillin-resistant *Staphylococcus aureus* therapy: past, present, and future. *Clin. Infect. Dis.* **2014**, *58*, S20–S27.
- (20) Chaudhuri, R. R.; Allen, A. G.; Owen, P. J.; Shalom, G.; Stone, K.; Harrison, M.; Burgis, T. A.; Lockyer, M.; Garcia-Lara, J.; Foster, S. J.; et al. Comprehensive identification of essential *Staphylococcus aureus* genes using Transposon-Mediated Differential Hybridisation (TMDH). *BMC Genom.* **2009**, *10*, 291.
- (21) Gallagher, L. A.; Ramage, E.; Weiss, E. J.; Radey, M.; Hayden, H. S.; Held, K. G.; Huse, H. K.; Zurawski, D. V.; Brittnacher, M. J.; Manoil, C. Resources for Genetic and Genomic Analysis of Emerging Pathogen *Acinetobacter baumannii*. *J. Bacteriol.* **2015**, *197* (12), 2027–2035.
- (22) Lewin, G. R.; Stacy, A.; Michie, K. L.; Lamont, R. J.; Whiteley, M. Large-scale identification of pathogen essential genes during coinfection with sympatric and allopatric microbes. *Proc. Natl. Acad. Sci. U.S.A.* **2019**, *116* (39), 19685–19694.
- (23) Mulani, M. S.; Kamble, E. E.; Kumkar, S. N.; Tawre, M. S.; Pardesi, K. R. Emerging Strategies to Combat ESKAPE Pathogens in the Era of Antimicrobial Resistance: A Review. *Front. Microbiol.* **2019**, *10*, 539.
- (24) Persyn, E.; Sassi, M.; Aubry, M.; Broly, M.; Delanou, S.; Asehnoune, K.; Caroff, N.; Crémet, L. Rapid genetic and phenotypic changes in *Pseudomonas aeruginosa* clinical strains during ventilator-associated pneumonia. *Sci. Rep.* **2019**, *9* (1), 4720.
- (25) Ramage, B.; Erolin, R.; Held, K.; Gasper, J.; Weiss, E.; Brittnacher, M.; Gallagher, L.; Manoil, C. Comprehensive Arrayed Transposon Mutant Library of *Klebsiella pneumoniae* Outbreak Strain KPNIH1. *J. Bacteriol.* **2017**, *199* (20), 10.
- (26) Johnson, S. M.; Sharif, O.; Mak, P. A.; Wang, H. T.; Engels, I. H.; Brinker, A.; Schultz, P. G.; Horwich, A. L.; Chapman, E. A biochemical screen for GroEL/GroES inhibitors. *Bioorg. Med. Chem. Lett.* **2014**, *24* (3), 786–789.

- (27) Sivinski, J.; Ambrose, A. J.; Panfilenko, I.; Zerio, C. J.; Machulis, J. M.; Mollasalehi, N.; Kaneko, L. K.; Stevens, M.; Ray, A. M.; Park, Y.; et al. Functional Differences between *E. coli* and ESKAPE Pathogen GroES/GroEL. *mBio* **2021**, *12* (1), 1–16.
- (28) Sivinski, J.; Ngo, D.; Zerio, C. J.; Ambrose, A. J.; Watson, E. R.; Kaneko, L. K.; Kostelic, M. M.; Stevens, M.; Ray, A.; Park, Y.; et al. Allosteric differences dictate GroEL complementation of *E. coli*. *Faseb. J.* **2022**, *36* (3), No. e22198.
- (29) Kostelic, M. M.; Zak, C. K.; Liu, Y.; Chen, V. S.; Wu, Z.; Sivinski, J.; Chapman, E.; Marty, M. T. UniDecCD: Deconvolution of Charge Detection-Mass Spectrometry Data. *Anal. Chem.* **2021**, *93* (44), 14722–14729.
- (30) Marty, M. T.; Baldwin, A. J.; Marklund, E. G.; Hochberg, G. K. A.; Benesch, J. L. P.; Robinson, C. V. Bayesian deconvolution of mass and ion mobility spectra: from binary interactions to polydisperse ensembles. *Anal. Chem.* **2015**, *87* (8), 4370–4376.
- (31) Washburn, A.; Abdeen, S.; Ovechkina, Y.; Ray, A. M.; Stevens, M.; Chitre, S.; Sivinski, J.; Park, Y.; Johnson, J.; Hoang, Q. Q.; et al. Dual-targeting GroEL/ES chaperonin and protein tyrosine phosphatase B (PtpB) inhibitors: A polypharmacology strategy for treating *Mycobacterium tuberculosis* infections. *Bioorg. Med. Chem. Lett.* **2019**, *29* (13), 1665–1672.
- (32) Bandyopadhyay, B.; Goldenzweig, A.; Unger, T.; Adato, O.; Fleishman, S. J.; Unger, R.; Horovitz, A. Local energetic frustration affects the dependence of green fluorescent protein folding on the chaperonin GroEL. *J. Biol. Chem.* **2017**, *292* (50), 20583–20591.
- (33) Bandyopadhyay, B.; Mondal, T.; Unger, R.; Horovitz, A. Contact Order Is a Determinant for the Dependence of GFP Folding on the Chaperonin GroEL. *Biophys. J.* **2019**, *116* (1), 42–48.
- (34) Tikhonova, E. B.; Zgurskaya, H. I. AcrA, AcrB, and TolC of *Escherichia coli* Form a Stable Intermembrane Multidrug Efflux Complex. *J. Biol. Chem.* **2004**, *279* (31), 32116–32124.
- (35) Yu, E. W.; McDermott, G.; Zgurskaya, H. I.; Nikaido, H.; Koshland, D. E., Jr. Structural basis of multiple drug-binding capacity of the AcrB multidrug efflux pump. *Science* **2003**, *300* (5621), 976–980.
- (36) Munoz, K. A.; Hergenrother, P. J. Facilitating Compound Entry as a Means to Discover Antibiotics for Gram-Negative Bacteria. *Acc. Chem. Res.* **2021**, *54* (6), 1322–1333.
- (37) Richter, M. F.; Drown, B. S.; Riley, A. P.; Garcia, A.; Shirai, T.; Svec, R. L.; Hergenrother, P. J. Predictive compound accumulation rules yield a broad-spectrum antibiotic. *Nature* **2017**, *545* (7654), 299–304.
- (38) Herzik, M. A., Jr. Setting Up Parallel Illumination on the Talos Arctica for High-Resolution Data Collection. *Methods Mol. Biol.* **2021**, *2215*, 125–144.
- (39) Cheng, A.; Negro, C.; Bruhn, J. F.; Rice, W. J.; Dallakyan, S.; Eng, E. T.; Waterman, D. G.; Potter, C. S.; Carragher, B. Legion: New features and applications. *Protein Sci.* **2021**, *30* (1), 136–150.
- (40) Tegunov, D.; Cramer, P. Real-time cryo-electron microscopy data preprocessing with Warp. *Nat. Methods* **2019**, *16* (11), 1146–1152.
- (41) Punjani, A.; Rubinstein, J. L.; Fleet, D. J.; Brubaker, M. A. cryoSPARC: algorithms for rapid unsupervised cryo-EM structure determination. *Nat. Methods* **2017**, *14* (3), 290–296.
- (42) Smart, O. S.; Womack, T. O.; Sharff, A.; Flensburg, C.; Keller, P.; Paciorek, W.; Vonrhein, C.; Bricogne, G., *Grade*, version 1.2.20; Global Phasing Ltd.: Cambridge, United Kingdom, 2011. <https://www.globalphasing.com> (accessed 21 May, 2024).
- (43) Afonine, P. V.; Poon, B. K.; Read, R. J.; Sobolev, O. V.; Terwilliger, T. C.; Urzhumtsev, A.; Adams, P. D. Real-space refinement in PHENIX for cryo-EM and crystallography. *Acta Crystallogr., Sect. D: Struct. Biol.* **2018**, *74* (6), 531–544.
- (44) Emsley, P.; Cowtan, K. Coot: model-building tools for molecular graphics. *Acta Crystallogr. Sect. D Biol. Crystallogr.* **2004**, *60* (12), 2126–2132.
- (45) Goddard, T. D.; Huang, C. C.; Meng, E. C.; Pettersen, E. F.; Couch, G. S.; Morris, J. H.; Ferrin, T. E. UCSF ChimeraX: Meeting modern challenges in visualization and analysis. *Protein Sci.* **2018**, *27* (1), 14–25.
- (46) Schmidt, C. M.; Shis, D. L.; Nguyen-Huu, T. D.; Bennett, M. R. Stable maintenance of multiple plasmids in *E. coli* using a single selective marker. *ACS Synth. Biol.* **2012**, *1* (10), 445–450.
- (47) Thomason, L. C.; Costantino, N.; Court, D. L. *E. coli* genome manipulation by P1 transduction. *Curr. Protoc. Mol. Biol.* **2007**, *79*, 1 17 1–117 8.
- (48) Liu, H.; Naismith, J. H. An efficient one-step site-directed deletion, insertion, single and multiple-site plasmid mutagenesis protocol. *BMC Biotechnol.* **2008**, *8*, 91.